Effects of Non-Integral Number of Peristaltic Waves Transporting Couple Stress Fluids in Finite Length Channels

Sanjay Kumar Pandey and Dharmendra Tripathi

Department of Applied Mathematics, Institute of Technology, Banaras Hindu University, Varanasi-221005, India

Reprint requests to S. K. P.; E-mail: skpandey.apm@itbhu.ac.in or
D. T.; E-mail: dtripathi.rs.apm@itbhu.ac.in

Z. Naturforsch. **66a,** 172 – 180 (2011); received January 12, 2010 / revised September 9, 2010

Peristaltic flow of couple stress fluids is studied here in a finite length channel. The analysis is carried out under the assumption of long wavelength and low Reynolds number approximations. When the couple stress parameter increases, it is found that pressure diminishes, maximum averaged flow rate increases, mechanical efficiency decreases, area experiencing reflux reduces, and trapped bolus-size increases. A comparative study of integral and non-integral number of waves propagating along the channel is also done.

Key words: Peristaltic Transport; Couple Stress Fluid; Mechanical Efficiency; Reflux Limit; Trapping Limit.

1. Introduction

A couple stress fluid is a non-Newtonian fluid whose particle-size is taken into consideration during flow. Since the classical continuum theory ignores the particle-size effects, a micro-continuum theory propounded by Stokes [1] has been considered to take into account the particle size effects. The Stokes micro-continuum theory is the generalization of the classical theory of fluids. The polar effects such as the presence of couple stresses, body couples, and an anti-symmetric stress tensor are taken into consideration in it. In this model, the couple stress effects are considered as a consequence of the action of a deforming body on its neighbourhood. Blood, polymers, colloidal solutions etc. are couple stress fluids. The fluid flowing in the oesophagus is generally a colloidal solution. We plan to investigate peristaltic transport of a couple-stress fluid in a channel of finite length that can model the aforementioned flow in the oesophagus as well as the flow of a colloidal solution in a mechanical pump of finite length.

Peristalsis is a mechanism of pumping process in which a piston is not used. From biological point of view, it is a continuous wave-like muscle contraction and relaxation of the vessels. For instance, food bolus through oesophagus, chyme through duodenum, urine in ureters, and blood through blood vessels, roller pumps etc. are driven by peristaltic waves. The assumption of finite length helps us to study the propagation of a non-integral number of waves propagating along the channel.

In a short communication, Srivastava [2] reported that pressure increases as the couple stress parameter decreases in a tube. For a couple stress fluid pressure is more than that for Newtonian fluids. Some authors [3 – 6] further reported about peristaltic flow of couple stress fluids through different geometries of wall surfaces. They have all discussed the effects of the couple stress parameter or the magnetic field on pressure and friction force etc. of the fluid flowing in infinite length channels or tubes. However, physiological vessels such as oesophagus are of finite length in comparison to their width/diameter. Finiteness of length gives rise to a situation when a non-integral number of waves propagate along the walls and consequently a non-integral number of fluid-boluses are trapped at a particular instant. Such a situation never arises in an infinite length tube. This situation was investigated by Li and Brasseur [7] for Newtonian fluids. Misra and Pandey [8] and Pandey and Tripathi [9, 10] extended the results for power law, magneto hydro dynamic (MHD) and Maxwell fluids, respectively. We intend to discover these aspects for couple stress fluids flowing in channels.

0932–0784 / 11 / 0100–0172 $ 06.00 © 2011 Verlag der Zeitschrift für Naturforschung, Tübingen · http://znaturforsch.com

2. Mathematical Model

The wave propagating along the channel walls is mathematically modeled as

$$\tilde{h}(\tilde{\xi},\tilde{t}) = a - \tilde{\phi}\cos^2\frac{\pi}{\lambda}(\tilde{\xi} - c\tilde{t}), \tag{1}$$

where $\tilde{h}$, $\tilde{\xi}$, $\tilde{t}$, a, $\tilde{\phi}$, λ, and c represent the transverse vibration of the wall, the axial coordinate, time, the half width of the channel, the amplitude of the wave, the wavelength, and the wave velocity, respectively.

Neglecting the body forces and the body couples, the continuity equation and the equations of motion of couple stress fluids are given by

$$\frac{\partial\tilde{u}}{\partial\tilde{\xi}} + \frac{\partial\tilde{v}}{\partial\tilde{\eta}} = 0, \tag{2}$$

$$\rho\left(\frac{\partial\tilde{u}}{\partial\tilde{t}} + \tilde{u}\frac{\partial\tilde{u}}{\partial\tilde{\xi}} + \tilde{v}\frac{\partial\tilde{u}}{\partial\tilde{\eta}}\right) = -\frac{\partial\tilde{p}}{\partial\tilde{\xi}} + \mu\nabla^2\tilde{u} - \mu_1\nabla^4\tilde{u}, \tag{3}$$

$$\rho\left(\frac{\partial\tilde{u}}{\partial\tilde{t}} + \tilde{u}\frac{\partial\tilde{v}}{\partial\tilde{\xi}} + \tilde{v}\frac{\partial\tilde{v}}{\partial\tilde{\eta}}\right) = -\frac{\partial\tilde{p}}{\partial\tilde{\eta}} + \mu\nabla^2\tilde{v} - \mu_1\nabla^4\tilde{v}, \tag{4}$$

where ρ, $\tilde{u}$, $\tilde{v}$, $\tilde{\eta}$, $\tilde{p}$, μ, μ_1 are the fluid density, axial velocity, transverse velocity, transverse coordinate, pressure, viscosity, constant associated with couple stress, and

$$\nabla^2 \equiv \frac{\partial^2}{\partial\tilde{\xi}^2} + \frac{\partial^2}{\partial\tilde{\eta}^2}, \quad \nabla^4 = \nabla^2\nabla^2.$$

Introducing the following dimensionless parameters

$$\begin{aligned} &\xi = \frac{\tilde{\xi}}{\lambda}, \quad \eta = \frac{\tilde{\eta}}{a}, \quad u = \frac{\tilde{u}}{c}, \quad v = \frac{\tilde{v}}{c\delta}, \\ &\phi = \frac{\tilde{\phi}}{a}, \quad h = \frac{\tilde{h}}{a}, \quad p = \frac{\tilde{p}a^2}{\mu c\lambda}, \quad \mathrm{Re} = \frac{\rho ca}{\mu}, \\ &\delta = \frac{a}{\lambda}, \quad \alpha = a\sqrt{\frac{\mu}{\mu_1}}, \end{aligned} \tag{5}$$

where δ, Re, α are the wave number, Reynolds number, couple stress parameter, respectively, and applying the long wavelength and low Reynolds number approximation in (2)–(4), we get

$$\frac{\partial u}{\partial\xi} + \frac{\partial v}{\partial\eta} = 0, \tag{6}$$

$$\frac{\partial p}{\partial\xi} = \frac{\partial^2 u}{\partial\eta^2} - \frac{1}{\alpha^2}\frac{\partial^4 u}{\partial\eta^4}, \tag{7}$$

$$\frac{\partial p}{\partial\eta} = 0. \tag{8}$$

The boundary conditions are

$$\text{no slip condition: } u = 0 \text{ at } \eta = h, \qquad \text{regularity condition: } \frac{\partial u}{\partial\eta} = 0 \text{ at } \eta = 0, \tag{9}$$

vanishing of couple stresses:

$$\frac{\partial^2 u}{\partial\eta^2} = 0 \text{ at } \eta = h, \quad \frac{\partial^3 u}{\partial\eta^3} = 0 \text{ at } \eta = 0, \tag{10}$$

transverse velocity at the wall:

$$v = \frac{\partial h}{\partial t} \text{ at } \eta = h, \quad v = 0 \text{ at } \eta = 0. \tag{11}$$

Equation (7) under the boundary conditions (9) and (10), yields the axial velocity

$$u = \frac{\partial p}{\partial\xi}\left[\frac{1}{2}(\eta^2 - h^2) + \frac{1}{\alpha^2}\left\{1 - \frac{\cosh(\alpha\eta)}{\cosh(\alpha h)}\right\}\right]. \tag{12}$$

Using (12) and the second condition of (11), the transverse velocity is obtained as

$$\begin{aligned} v = {} & \frac{\partial p}{\partial\xi}\frac{\partial h}{\partial\xi}\left\{h\eta + \frac{\sinh(\alpha\eta)\,\mathrm{sech}(\alpha h)\tanh(\alpha h)}{\alpha^2}\right\} \\ & -\frac{\partial^2 p}{\partial\xi^2}\left\{\frac{1}{6}(\eta^3 - 3h^2\eta) + \frac{1}{\alpha^2}\left(\eta - \frac{\sinh(\alpha\eta)}{\alpha\cosh(\alpha h)}\right)\right\}. \end{aligned} \tag{13}$$

The transverse velocity, at the boundary of wall, is obtained by substituting the first condition of (11) into (13). It yields

$$\begin{aligned} \frac{\partial h}{\partial t} = {} & \frac{\partial p}{\partial\xi}\frac{\partial h}{\partial\xi}\left\{h^2 + \frac{1}{\alpha^2\tanh^2(\alpha h)}\right\} \\ & + \frac{\partial^2 p}{\partial\xi^2}\left(\frac{h^3}{3} + \frac{1}{\alpha^3}(\tanh(\alpha h) - \alpha h)\right). \end{aligned} \tag{14}$$

Integrating (14) once with respect to ξ, the pressure gradient across the length of the channel is obtained as

$$\frac{\partial p}{\partial\xi} = \frac{3\alpha^3\left(G(t) + \int_0^\xi \frac{\partial h}{\partial t}\mathrm{d}\xi\right)}{\alpha^3h^3 + 3(\tanh(\alpha h) - \alpha h)}, \tag{15}$$

where $G(t)$ is a function of t.

Further, integrating (15) from 0 to ξ, the pressure difference is obtained as

$$\begin{aligned} & p(\xi,t) - p(0,t) = \\ & 3\alpha^3\int_0^\xi \frac{\left(G(t) + \int_0^s \frac{\partial h}{\partial t}\mathrm{d}s_1\right)}{\alpha^3h^3 + 3(\tanh(\alpha h) - \alpha h)}\mathrm{d}s. \end{aligned} \tag{16}$$

The substitution $\xi = l$ in (16) readily gives the pressure difference between inlet and outlet of the channel as

$$p(l,t) - p(0,t) = 3\alpha^3 \int_0^l \frac{\left(G(t) + \int_0^\xi \frac{\partial h}{\partial t} \mathrm{d}s\right)}{\alpha^3 h^3 + 3(\tanh(\alpha h) - \alpha h)} \mathrm{d}\xi, \tag{17}$$

from which $G(t)$ is evaluated as

$$G(t) = \frac{\frac{p(l,t)-p(0,t)}{3\alpha^3} - \int_0^l \frac{\int_0^\xi \frac{\partial h}{\partial t}\mathrm{d}s}{\alpha^3 h^3 + 3(\tanh(\alpha h) - \alpha h)} \mathrm{d}\xi}{\int_0^l \frac{1}{\alpha^3 h^3 + 3(\tanh(\alpha h) - \alpha h)} \mathrm{d}\xi}. \tag{18}$$

The instantaneous volume flow rate in the laboratory frame is defined as $Q(\xi,t) = \int_0^h u \mathrm{d}y$, which, by virtue of (12), assumes the following form:

$$Q(\xi,t) = -\frac{\partial p}{\partial \xi} \frac{\alpha^3 h^3 + 3(\tanh(\alpha h) - \alpha h)}{3\alpha^3}. \tag{19}$$

When averaged over one time period, it gives

$$\begin{aligned} \bar{Q} &= \int_0^1 Q(\xi,t) \mathrm{d}t \\ &= -\frac{1}{3\alpha^3} \int_0^1 \frac{\partial p}{\partial \xi} (\alpha^3 h^3 + 3(\tanh(\alpha h) - \alpha h)) \mathrm{d}t. \end{aligned} \tag{20}$$

But, the following are the existing relations between the averaged flow rate and flow rate in the wave frame and in laboratory frame:

$$\bar{Q} = q + 1 - \frac{\phi}{2} = Q - h + 1 - \frac{\phi}{2}. \tag{21}$$

A simple manipulation of (19), followed by the application of (21), yields the pressure gradient as

$$\frac{\partial p}{\partial \xi} = -\frac{3\alpha^3 \left(\bar{Q} + h - 1 + \frac{\phi}{2}\right)}{\alpha^3 h^3 + 3(\tanh(\alpha h) - \alpha h)}, \tag{22}$$

which, on integrating between 0 and ξ, gives

$$p(\xi) - p(0) = -3\alpha^3 \int_0^\xi \frac{\left(\bar{Q} + h - 1 + \frac{\phi}{2}\right)}{\alpha^3 h^3 + 3(\tanh(\alpha h) - \alpha h)} \mathrm{d}s. \tag{23}$$

The local wall shear stress defined as $\tau_\mathrm{w} = \left.\frac{\partial u}{\partial \eta}\right|_{\eta=h}$ reduces, by virtue of (12) and (15), to

$$\tau_\mathrm{w} = \frac{3\alpha^2(\alpha h - \tanh(\alpha h))\left(G(t) + \int_0^\xi \frac{\partial h}{\partial t}\mathrm{d}s\right)}{\alpha^3 h^3 + 3(\tanh(\alpha h) - \alpha h)}. \tag{24}$$

Mechanical efficiency (cf. [11]) is derived for couple stress fluids as

$$E = \frac{\bar{Q}\Delta p_1}{\phi(I_1 - \Delta p_1)}, \tag{25}$$

where $I_1 = \int_0^1 \frac{\partial p}{\partial \xi} \cos(2\pi\xi)\mathrm{d}\xi$, and Δp_1 is the pressure difference across a wavelength, which, by using the (23), becomes

$$\Delta p_1 = p(1) - p(0) = -3\alpha^3 \int_0^1 \frac{\left(\bar{Q} + h - 1 + \frac{\phi}{2}\right)}{\alpha^3 h^3 + 3(\tanh(\alpha h) - \alpha h)} \mathrm{d}\xi. \tag{26}$$

Moreover, the maximum flow rate is obtained by substituting $\Delta p_1 = 0$ as

$$\bar{Q}_0 = 1 - \frac{\phi}{2} - \frac{\int_0^1 \frac{h}{\alpha^3 h^3 + 3(\tanh(\alpha h) - \alpha h)} \mathrm{d}\xi}{\int_0^1 \frac{1}{\alpha^3 h^3 + 3(\tanh(\alpha h) - \alpha h)} \mathrm{d}\xi}. \tag{27}$$

Reflux (cf. [11]) is an important phenomenon of peristaltic movement. The dimensional form of the stream function in the wave frame is defined as

$$\mathrm{d}\tilde{\psi} = \tilde{U}\mathrm{d}\tilde{Y} - \tilde{V}\mathrm{d}\tilde{X}, \tag{28}$$

where $\tilde{\psi}$, $\tilde{Y}$, $\tilde{X}$, $\tilde{U}$, and $\tilde{V}$ are the stream function, coordinates, and velocities components, respectively. Using the transformations between wave and laboratory frame, defined as

$$\begin{aligned} &\tilde{X} = \tilde{\xi} - c\tilde{t}, \quad \tilde{Y} = \tilde{\eta}, \quad \tilde{U} = \tilde{u} - c, \\ &V = v, \quad \tilde{q} = \tilde{Q} - c\tilde{h}, \end{aligned} \tag{29}$$

where the parameters on the left side are in the wave frame and that on the right side are in the laboratory frame. We obtain the stream function by solving (12), (13), and (28) in the form

$$\psi = -\left[\frac{\bar{Q} - 1 + \frac{\phi}{2} + h}{\alpha^3 h^3 + 3(\tanh(\alpha h) - \alpha h)} \left\{\frac{\alpha^3}{2}(\eta^3 - 3h^2\eta) + 3\left(\alpha\eta - \frac{\sinh(\alpha\eta)}{\cosh(\alpha h)}\right)\right\} + \eta\right]. \tag{30}$$

At the wall

$$\psi\big|_{\eta=h} = \psi_{\mathrm{w}} = \bar{Q} - 1 + \frac{\phi}{2}. \tag{31}$$

When averaged for one cycle, the reflux flow rate $Q_{\psi}(\xi) = \psi + \eta(\psi,\xi)$ yields

$$\bar{Q}_{\psi} = \psi + \int_0^1 \eta(\psi,\xi)\mathrm{d}\xi. \tag{32}$$

To evaluate the reflux limit, $\bar{Q}_{\psi}$ is expanded in power series in terms of a small parameter ε about the wall, where $\varepsilon = \psi - \psi_{\mathrm{w}}$ and is subjected to the reflux condition

$$\frac{\bar{Q}_{\psi}}{\bar{Q}} > 1 \ \text{ as } \ \varepsilon \to 0. \tag{33}$$

The coefficients of the first two terms in the expansion $\eta = h + a_1\varepsilon + a_2\varepsilon^2 + \cdots$ are found for small value of α by using (30) as

$$\begin{aligned} a_1 &= -1, \\ a_2 &= \frac{3\alpha^3 h(1-\cosh(\alpha h))}{2\cosh(\alpha h)} \\ &\quad \cdot \frac{\bar{Q} - 1 + \frac{\phi}{2} + h}{\alpha^3 h^3 + 3(\tanh(\alpha h) - \alpha h)}. \end{aligned} \tag{34}$$

Integrating (32), and substituting the coefficients from (34), the reflux limit is obtained, for couple stress fluids, as

$$\begin{aligned} \bar{Q} < 1 - \frac{\phi}{2} \\ - \frac{\displaystyle\int_0^1 \frac{h^2(1-\cosh(\alpha h))}{\cosh(\alpha h)[\alpha^3 h^3 + 3(\tanh(\alpha h) - \alpha h)]}\mathrm{d}\xi}{\displaystyle\int_0^1 \frac{h(1-\cosh(\alpha h))}{\cosh(\alpha h)[\alpha^3 h^3 + 3(\tanh(\alpha h) - \alpha h)]}\mathrm{d}\xi}. \end{aligned} \tag{35}$$

3. Numerical Results and Discussion

3.1. Numerical Aspects

This section presents the salient features of couple stress parameter on pressure distribution, i. e., $p(\xi,t) - p(0,t)$, local wall shear stress τ_{w}, averaged flow rate $\bar{Q}$, maximum averaged flow rate $\bar{Q}_0$, mechanical efficiency E, reflux limit, and trapping through Figures 1 – 7. Numerical results have been obtained by writing programmes in C-language applying numerical techniques (e. g., Simpson's rule for integration).

In order to carry out the computer simulation of the model, we consider the propagation of integral number and non-integral number of waves in a train along the walls of a channel. To this end, we consider the simplest case known as free pumping, i. e., the pressures at the two ends of the channel are zero, i. e., $p(l,t) = p(0,t) = 0$.

In order to investigate the temporal dependence of pressure on the axial distance we plot graphs (Figs. 1a – d) at various instants $t = 0 - 1$ with an interval of 0.25 with couple stress parameter α varying from 4 – 10 based on (16) in conjunction with (18). We consider a train wave propagation (in particular, two waves in the train) on the walls of the channel.

It is observed that for $t = 0$ (Fig. 1a), the pressure at the inlet is large. The pressure is at its maximum, i. e., peak near the tail of the bolus, and then there is a sharp nonlinear decline of pressure to zero at the middle, which further diminishes to its minimum, i. e., trough. Then the pressure rises very sharply and linearly, almost vertically, to zero at the head of the bolus and maintains the same trend to reach another maximum, i. e., peak equal to the previous maximum one. The pressure distribution for the leading bolus is identical and the final pressure at the head of the leading bolus is zero. For $t = 0.25 - 0.75$ revealed by Figures 1b – d, the pressure distributions depict a continuous process of bolus movement from the one end to another end of the channel with similar peaks and troughs. When $t = 1.0$, the pressure distribution is identical with that for $t = 0$. Finally, it is observed that the pressure diminishes with the increase in the magnitude of the couple stress parameter.

Figures 2a – d display the propagation of a non-integral number of waves in the train, which is an inherent feature of finite length vessels. In this case, we take $l = 1.8$. The effect of the couple stress parameter on the pressure difference in both cases is similar, but a significant difference between the two is that the peaks of pressure for the two boluses are identical in the integral case while the peaks are different in the non-integral case.

Figures 3a – d present the influence of couple stress parameter on local wall shear stress along the length of the channel. It is observed that the local wall shear stress bears similarity with the pressure distribution at various instants and range between peak and trough decreases when the magnitude of the couple stress parameter increases.

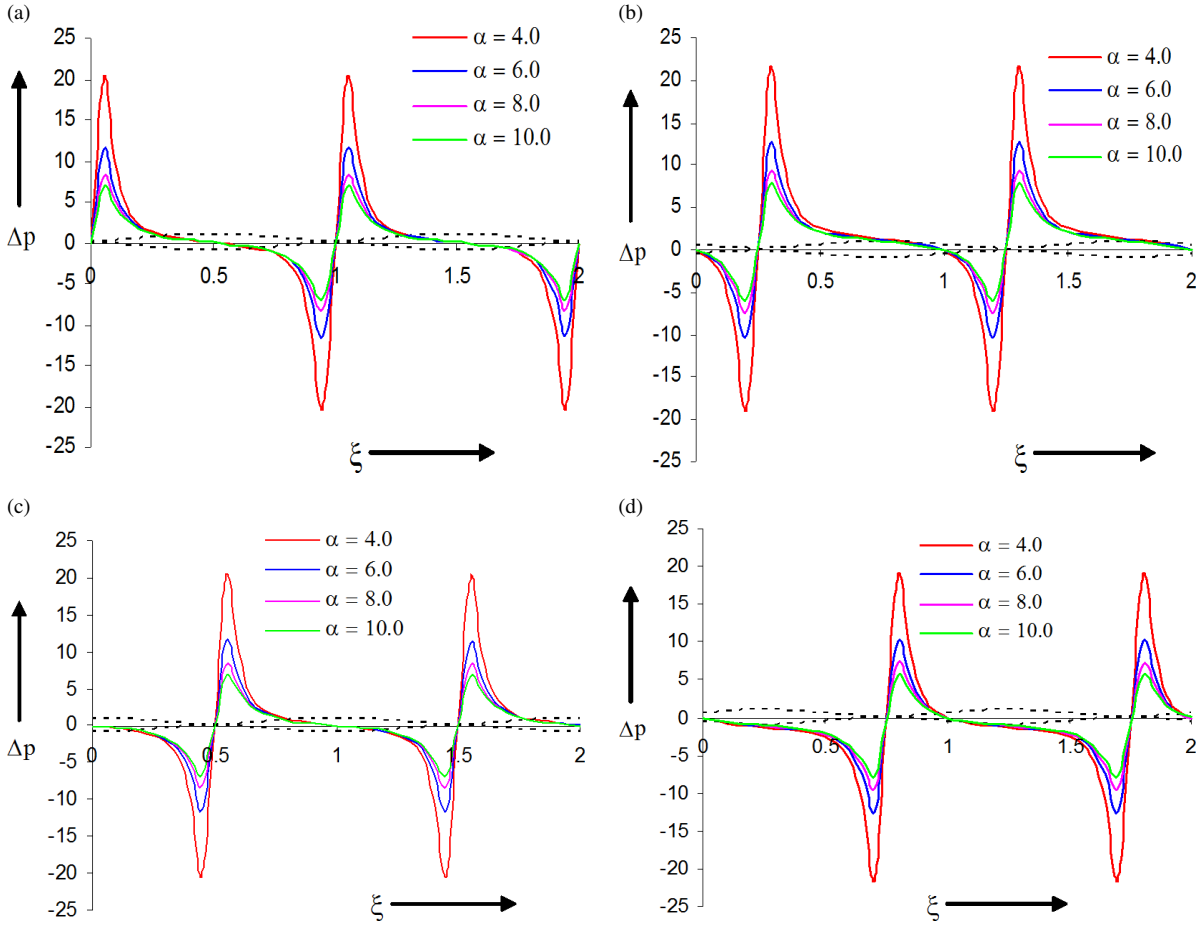

Fig. 1 (colour online). Pressure vs. axial distance at $\alpha = 4.0, 6.0, 8.0, 10.0$, $\phi = 0.9$, $l = 2.0$ and various instants (a) $t = 0.0$, 1.0, (b) $t = 0.25$, (c) $t = 0.5$, (d) $t = 0.75$. Dotted lines represent the position of wave and colour solid lines show pressure along the length of channel.

Figure 4 depicts the variation of the pressure across one wavelength Δp_1 against the averaged flow rate $\bar{Q}$ for different values of α at $\phi = 0.6$. It is observed that there is a linear relation between pressure and averaged flow rate. Also, an increase in the flow rate reduces the pressure and thus maximum flow rate is achieved at zero pressure and the maximum pressure occurs at zero averaged flow rates. It is also evident from the figure that the pressure decreases with increasing α.

Figure 5 is plotted for mechanical efficiency E vs. the ratio of averaged flow rate to maximum averaged flow rate $\bar{Q}/\bar{Q}_0$. There is a nonlinear relation between them. First E rises with $\bar{Q}/\bar{Q}_0$ from zero to the maximum value, thereafter it falls to zero. Finally, it reveals that the mechanical efficiency decreases with increasing α.

Figure 6 depicts the impact of couple stress parameter on the reflux limit. The upper portion of the curves is no reflux region while the lower portion is reflux region. It is observed that the reflux region decreases when α increases.

Figures 7a – d are drawn for streamlines in the wave frame for various values of $\alpha = 1.0$, 1.2, 1.3, 2.0 for $\bar{Q} = 0.5$ and $\phi = 0.5$. The figures show that the size of the trapped bolus increases and so trapping of the bolus reduces with increasing α.

3.2. Physical Interpretation and Physiological and Engineering Applications

The keen observation given in the fourth paragraph of Section 3.1 reveals many interesting facts of the

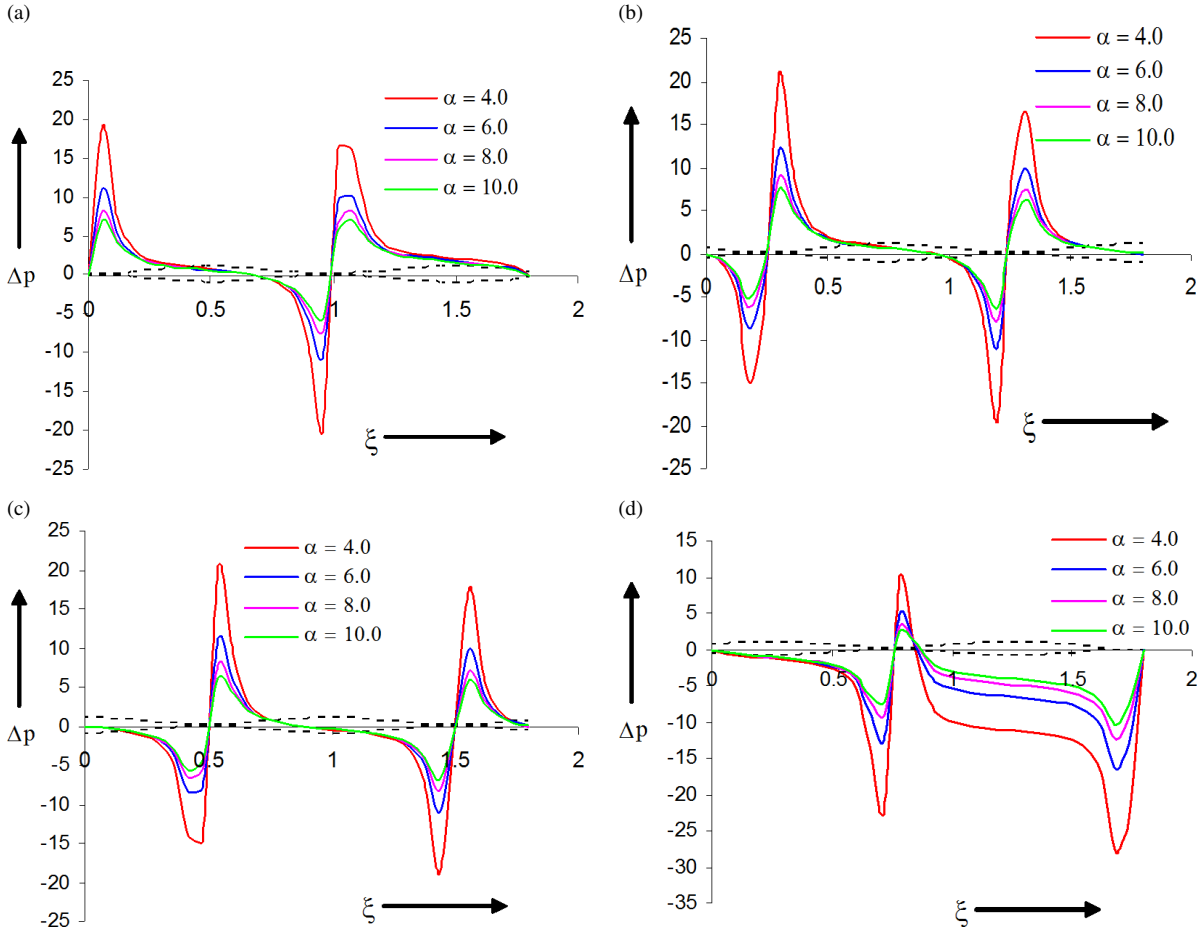

Fig. 2 (colour online). Pressure vs. axial distance at $\alpha = 4.0, 6.0, 8.0, 10.0$, $\phi = 0.9$, $l = 1.8$ and various instants (a) $t = 0.0$, 1.0, (b) $t = 0.25$, (c) $t = 0.5$, (d) $t = 0.75$. Dotted lines represent the position of wave and colour solid lines show pressure along the length of channel.

pumping mechanism for a safe smooth and harmonic motion in the oesophagus. Considering oesophagus as a channel and colloidal solutions swallowed in it as couple stress fluids and analyzing the numerical results displayed through the figures, the following inferences can be drawn.

Once a bolus has already entered into the oesophagus, the pressure at the inlet is initially large enough at its maximum value or the peak near the tail of the bolus to prevent a backward motion. In order to move it ahead it declines to zero at the middle of the bolus and further reaches the trough. In the meanwhile, the leading bolus has to be restrained from any possible backward motion; so it rises very sharply and linearly, almost vertically, to zero at the head of the trailing bolus which is also the tail of the leading bolus and maintains the same trend to reach another peak equal to the previous maximum one. The pressure distribution for the leading bolus is identical. It is observed that the final pressure at the head of the leading bolus is zero as desired. This rise of pressure to zero indicates a controlled motion of the bolus which is ready to be transported. At $t = 0.25$ a portion of a new bolus is in the process of transportation and one fourth of the leading bolus has already been transported. Similarly at $t = 0.5$ and $t = 0.75$, the pressure distributions depict a continuous harmonic process of bolus movement from the one end to another. The pressure distribution at $t = 1.0$ which is identical with that at $t = 0$ indicates that the pumping machinery is ready to repeat the process of transportation.

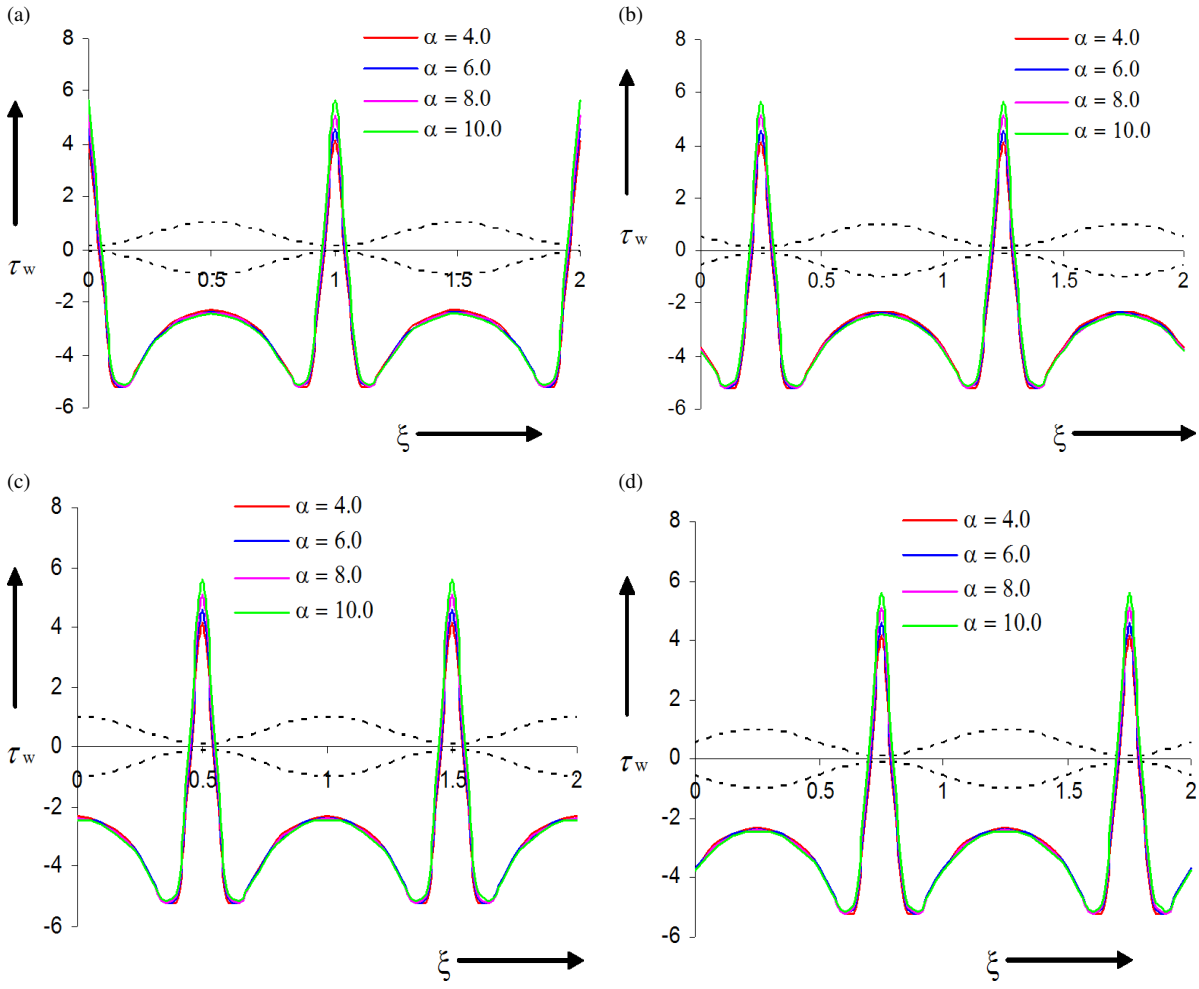

Fig. 3 (colour online). Local wall shear stress vs. axial distance at $\alpha = 4.0, 6.0, 8.0, 10.0$, $\phi = 0.9$, $l = 2.0$ and various instants (a) $t = 0.0, 1.0$, (b) $t = 0.25$, (c) $t = 0.5$, (d) $t = 0.75$. Dotted lines represent the position of wave and colour solid lines show local wall shear stress along the length of channel.

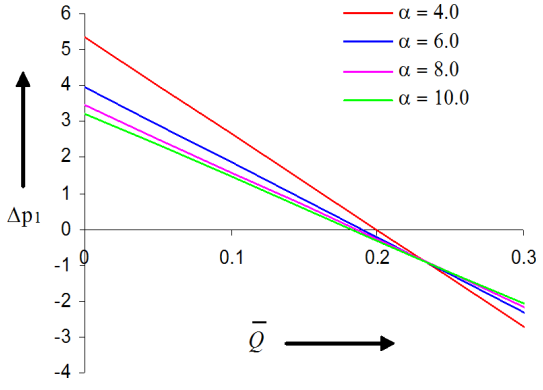

Fig. 4 (colour online). Pressure vs. averaged flow rate. Colour lines represent the pressure at fixed flow rate for $\alpha = 4.0, 6.0, 8.0, 10.0$ and $\phi = 0.6$.

Since the couple stress parameter $\alpha \to \infty$ makes the fluid Newtonian, the diminishing pressure with increasing couple stress parameter can be interpreted as that less pressure is required to transport Newtonian fluids compared with couple stress fluids.

Since the presence of a non-integral number of waves is an inherent characteristic of commercial pumps, the numerical results obtained for this case may be applied to commercial pumps. The different sizes of the peaks and troughs of pressure in the case of non-integral number of waves indicate that the mechanism may be similar but the pressure distributions in the two cases are distinct. This may be concluded that the pressure

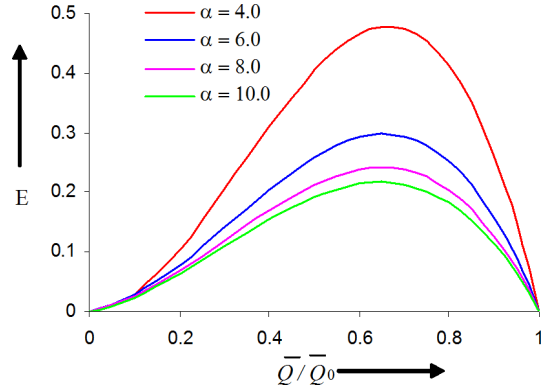

Fig. 5 (colour online). Mechanical efficiency vs. ratio of averaged flow rate and maximum averaged flow rate. Colour lines represent the efficiency of pump for $\alpha = 4.0$, 6.0, 8.0, 10.0 and $\phi = 0.6$.

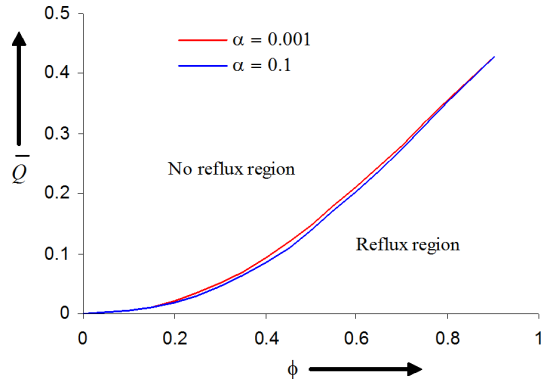

Fig. 6 (colour online). Averaged flow rate vs. amplitude. Colour lines represent reflux limit at $\alpha = 0.001$, 0.1.

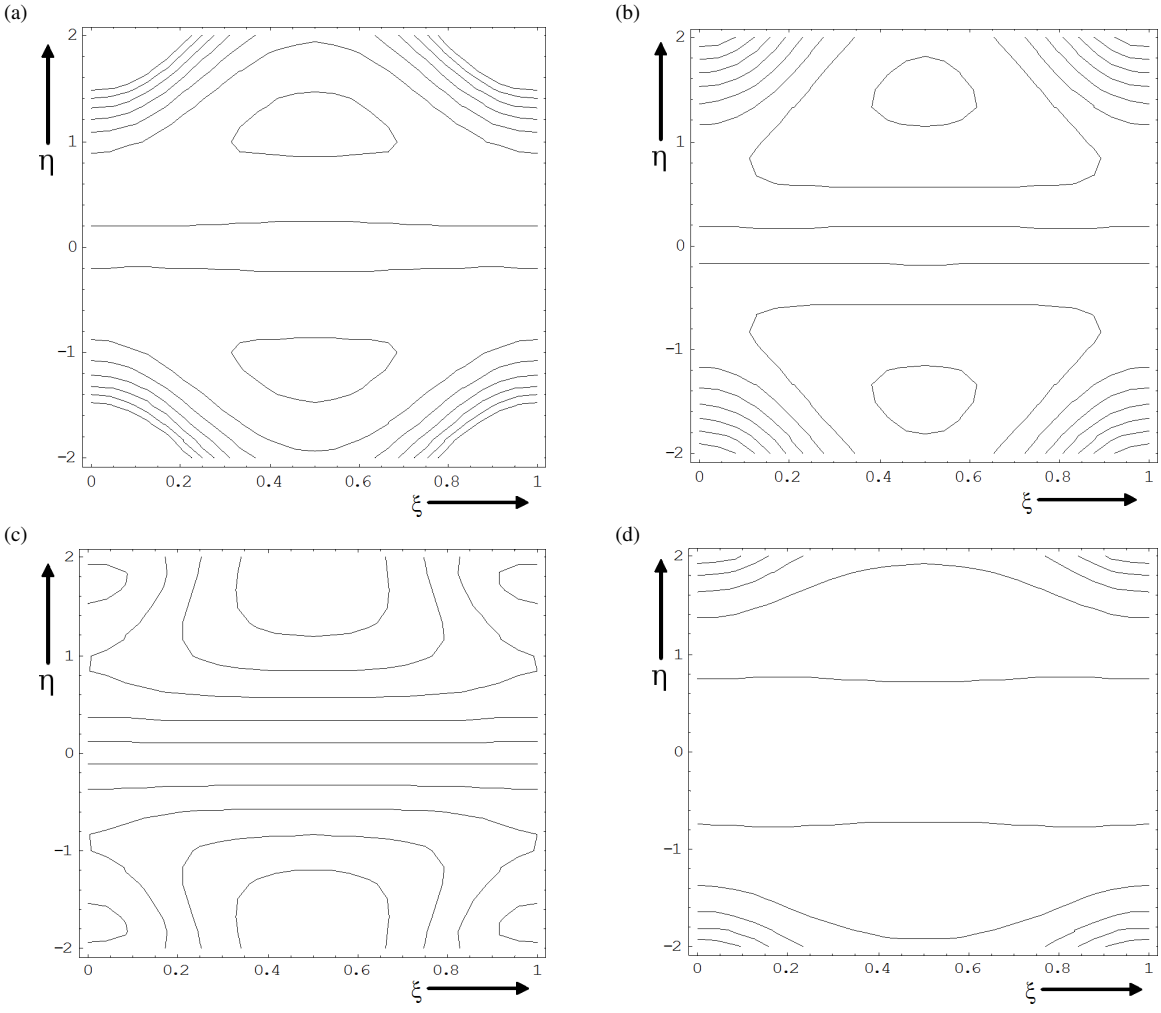

Fig. 7. Streamlines in the wave frame when (a) $\bar{Q} = 0.5$, $\phi = 0.5$, $\alpha = 1.0$, (b) $\bar{Q} = 0.5$, $\phi = 0.5$, $\alpha = 1.2$, (c) $\bar{Q} = 0.5$, $\phi = 0.5$, $\alpha = 1.3$, (d) $\bar{Q} = 0.5$, $\phi = 0.5$, $\alpha = 2.0$.

exerted on the fluid in such pumps is not as balanced as observed in natural pumps such as oesophagus.

It has also been found that mechanical efficiency decreases with increasing α. Thus for transporting a couple stress fluid the pump has to be more efficient. This endorses the conclusion drawn in the previous paragraph.

A decreasing reflux region with an increasing couple stress parameter indicates that the couple stress fluid is more prone to reflux.

A reduction of trapping with increasing α reveals that the couple stress fluid is more prone to trapping.

4. Concluding Remarks

It is found that the pressure diminishes with increasing couple stress parameter. The peaks of pressure for different boluses are identical in the integral case but different in the non-integral case. The curves for local wall shear stress are qualitatively similar, but quantitatively different for various values of couple stress parameter. Averaged flow rate decreases with the increase in pressure across one wavelength. The larger the couple stress parameter, the higher is the maximum averaged flow rate. Mechanical efficiency decreases with increasing couple stress parameter. The area experiencing reflux reduces with increasing couple stress parameter. The size of the trapped bolus increases with couple stress parameter.

[1] V. K. Stokes, Phys. Fluid **9**, 1709 (1966).
[2] L. M. Srivastava, Rheologica Acta **25**, 638 (1986).
[3] E. F. El Shehawey and W. El-Sebaei, Physica Scripta **64**, 401 (2001).
[4] Kh. S. Mekheimer, Phys. Lett. A **372**, 4271 (2008).
[5] N. Ali, T. Hayat, and M. Sajid, Biorheology, **44**, 125 (2007).
[6] A. M. Shobh, Turkish J. Eng. Env. Sci. **32**, 117 (2008).
[7] M. Li and J. G. Brasseur, J. Fluid Mech. **248**, 129 (1993).
[8] J. C. Misra and S. K. Pandey, Math. Comput. Model. **33**, 997 (2001).
[9] S. K. Pandey and D. Tripathi, Appl. Bionics Biomech. **7**, 169 (2010).
[10] S. K. Pandey and D. Tripathi, J. Biol. Syst. **18**, 621 (2010).
[11] A. H. Shapiro, M. Y. Jafferin, and S. L. Weinberg, J. Fluid Mech. **35**, 669 (1969).